Research Article Vol. 37, No. 4 / April 2020 / Journal of the Optical Society of America B 1219

Journal of the Optical Society of America B

OPTICAL PHYSICS

Efficient numerical model of stimulated Raman scattering in optical fibers

SERGEY SMIRNOV

Novosibirsk State University, Pirogova str., 2, Novosibirsk 630090, Russia (smirnov@lab.nsu.ru)

Received 17 January 2020; revised 5 March 2020; accepted 5 March 2020; posted 5 March 2020 (Doc. ID 387812); published 30 March 2020

The paper proposes a novel efficient numerical model for simulation of spectral and temporal transformation of laser pulses due to interplay of Kerr and Raman nonlinearity and chromatic dispersion in the process of propagation through single-mode optical fibers. The model reproduces qualitatively the spectral shape of Raman gain within the approximation of slowly varying amplitudes using a pair of meshes (for pump and Stokes waves) with a reduced number of points. Nonlinear propagation of 100-ps-long laser pulses along an optical fiber is used as a test bed for the new model. It is shown that the proposed model provides accuracy better than 10% in Stokes wave energy growth speed, while being up to eight times more efficient in memory usage and computation speed compared to the generalized nonlinear Schrödinger equation.

https://doi.org/10.1364/JOSAB.387812

1. INTRODUCTION

Various approaches are used for simulation of the Raman effect in optical fibers and lasers. The simplest and most cost-effective model is based on numerical solution of the equations for pump and Stokes intensity distributions along a fiber, $I_p(z)$ and $I_S(z)$: $I'_S = g_R I_p I_S - \alpha_S I_S$; $I'_p = -\frac{\omega_p}{\omega_S} g_R I_p I_S - \alpha_p I_p$, where g_R is the Raman-gain coefficient, $\omega_{S,p}$ stand for the wave frequencies, and $\alpha_{S,p}$ introduce fiber losses [1,2]. However, this approach provides information onlyabout the power of the pump and Stokes waves. In order to explore the spectral and temporal properties of optical waves, one can use the generalized nonlinear Schrödinger equation (GNLSE) [1,3]:

$$\partial_z A = -(\alpha_0 + i\alpha_1\partial_t)\frac{A}{2} - \frac{i\beta_2}{2}\partial_t^2 A + \frac{\beta_3}{6}\partial_t^3 A + i\gamma \times \left(1 + \frac{i\partial_t}{\omega_0}\right)\left(A\int_0^\infty R(t')|A(z, t-t')|^2 \mathrm{d}t'\right), \quad (1)$$

where $A(z, t)$ stands for the complex field envelope; z and t are the longitudinal coordinate and time in the retarded frame of reference, respectively; ω_0 stands for the carrier frequency; β_2 and γ are the dispersion and nonlinear coefficients, respectively; α_0 and α_1 are the first two coefficients in Taylor series expansion of the optical losses $\alpha(\omega)$ at $\omega = \omega_0$; c denotes the light speed in vacuum; and $i^2 = -1$. The kernel $R(t)$ of the integral operator includes both electronic (instantaneous) and nuclear contributions: $R(t) = (1 - f_R)\delta(t) + f_R h_R(t)$. Delayed (Raman) response of silica in the first approximation can be taken in the form of a damped oscillator:

$$h_R(t) = \frac{\tau_1^2 + \tau_2^2}{\tau_1 \tau_2^2} \cdot e^{-t/\tau_2} \sin\frac{t}{\tau_1}, \quad (2)$$

with time scales $\tau_1 = 12.2$ fs, $\tau_2 = 32$ fs, and delayed response fraction $f_R = 0.18$ [1,3].

Although Eq. (1) and its modifications are used widely for modeling ultra-short pulse propagation and supercontinuum generation [4–6], it may require a large amount of computational resources [6] in the case of long high-energy pulses with relatively narrow optical spectra that are common in long fiber lasers [7–13] and other pump sources used in Raman converters [14,15]. Intra-cavity dynamics and generation regimes of such lasers may be substantially affected by the Raman effect [16–20], therefore requiring development of more efficient numerical models. Thus, in order to simulate spectral Raman transformation of laser pulses that fit into $T = 5$ ns-wide mesh using Eq. (1), one must choose the number of mesh points as large as $N > T\Delta\nu_R \gtrsim 10^5$, where $\Delta\nu_R \approx 13$ THz is the Raman frequency shift for silica. In such a case, only a small fraction of the spectral mesh points is actually used, whereas spectral power at other points is vanishing, which makes the model based on Eq. (1) inefficient.

Much higher efficiency may be attained using a different approach that relies on a coupled set of GNLSEs [1,21] for two slowly varying complex amplitudes, one for the pump and another for the Stokes wave instead of a single amplitude for both waves. However, Raman gain of such a model is spectrally uniform, thus effectively constraining it to multipass Raman converters and Raman lasers with strong intra-cavity spectral shaping of the Stokes wave [14,22–25]. Such intra-cavity spectral shaping may also be implicit, e.g., in the case of chirped

Raman dissipative solitons (DSs) that experience amplification only when they overlap in time with the pumping DSs [26].

In this work, we report benchmark tests of our novel numerical model for simulation of spectral and temporal transformation of laser pulses propagating through single-mode optical fibers with Kerr and Raman nonlinearities and chromatic dispersion. The model is suitable for single-pass Raman converters and fiber lasers [14,15,27] and demonstrates high computational efficiency in the case of narrow optical spectra that occur in long fiber lasers generating high-energy pulses. Since the model is based on the approximation of slowly varying amplitudes, the spectral width of the pump wave must be much narrower than the Stokes frequency shift. In particular, the model is unlikely to provide much gain in computational efficiency in the case when the pump spectral width is comparable to the Stokes shift [28], and furthermore, it is obviously inapplicable in cases when the pump spectrum merges with the Raman peak [29], thus forming a continuous spectrum. In the following sections, we start with derivation of the underlying equations and then perform numerical tests of the new model in order to gain insight into its accuracy and efficiency. Finally, we summarize our findings and draw conclusions about applicability of the new model.

2. MODEL

Since the split-step Fourier method (SSFM) is a common choice for integration of GNLSE, it is convenient to rewrite Eq. (1) in the form $\partial_z A = \hat{D}A + \hat{N}A$, where $\hat{D}$ and $\hat{N}$ denote the dispersive and nonlinear terms of Eq. (1), respectively. In the case of slowly varying amplitudes (narrow optical spectrum), correction term $(i/\omega_0)\partial_t$ is much smaller than unity and thus can be omitted, so that $\hat{N}A = i\gamma(1-f_R)|A|^2A + i\gamma f_R A\int_0^\infty h_R(t')|A(t-t')|^2\mathrm{d}t'$. Let us make a substitution $A(z,t) = A_0(z,t) + A_1(z,t)e^{-i\omega_s t}$, where A_0 and A_1 are the slow amplitudes of the pump and Stokes waves, and $\omega_S/2\pi = -13$ THz is the Stokes shift for silica; then let us separately write down the terms that oscillate at zero frequency and at ω_S:

$$\hat{N}A_0 = i\gamma f_R\cdot\left(A_0\int_0^\infty h_R(t')\left[|A_0(t-t')|^2+|A_1(t-t')|^2\right]\mathrm{d}t' + A_1\int_0^\infty h_R(t')A_0(t-t')A_1^*(t-t')e^{-i\omega_S t'}\mathrm{d}t'\right) + i\gamma(1-f_R)(|A_0|^2+2|A_1|^2)A_0;$$

$$\hat{N}A_1 = i\gamma f_R\cdot\left(A_1\int_0^\infty h_R(t')\left[|A_0(t-t')|^2+|A_1(t-t')|^2\right]\mathrm{d}t' + A_0\int_0^\infty h_R(t')A_0^*(t-t')A_1(t-t')e^{i\omega_S t'}\mathrm{d}t'\right) + i\gamma(1-f_R)(|A_1|^2+2|A_0|^2A_0)A_1.$$

Slow amplitudes $A_{0,1}$ vary only slightly on the time scale τ_2, where $h_R(t')$ is essentially non-zero, and so can be treated as constants. However, this leads to a model with spectrally uniform gain [21]. Thus, we ought to consider small variation of slow amplitudes over time scale τ_2 by replacing $A_{0,1}$ by their Taylor series expansions inside the integrals: $A_{0,1}(t-t') \approx A_{0,1}(t) - t'\partial_t A_{0,1}(t)$. This leads us to

$$\hat{N}A_0 = i\gamma\{(|A_0|^2 + (2-f_R+f_Rc_1)|A_1|^2)A_0 - f_Rc_2(A_0\partial_t A_1^* + A_1^*\partial_t A_0)A_1\}, \tag{3}$$

$$\hat{N}A_1 = i\gamma\{(|A_1|^2 + (2-f_R+f_Rc_1^*)|A_0|^2)A_1 - f_Rc_2^*(A_0^*\partial_t A_1 + A_1\partial_t A_0^*)A_0\}, \tag{4}$$

where $c_{1,2}$ are complex coefficients defined as

$$c_1 = \int_0^\infty h_R(t')e^{i|\omega_S|t'}\mathrm{d}t', \quad c_2 = \int_0^\infty h_R(t')t'e^{i|\omega_S|t'}\mathrm{d}t'. \tag{5}$$

For response function (2), $c_1 = 0.2282 + 1.4486i$, and $c_2 = (-2.3712 + 49.479i)$ fs. It must be noted that in deriving Eqs. (3) and (4), we omitted the term $f_Rc_0\partial_t(|A_0|^2+|A_1|^2)$ with $c_0 = \int_0^\infty h_R(t')t'\mathrm{d}t' \approx 8.1$ fs, since it is much smaller than $|A_{0,1}|^2$ for pulses longer than 1 ps.

Let us also point out that since the time derivatives in Eqs. (3) and (4) appear as a result of Taylor series expansion of $A_{0,1}(t-t')$ at $t'>0$, one should apply non-symmetric finite-difference formulas in order to evaluate time derivatives $\partial_t A_{0,1}(t)$ to the left of point t. Thus, in the first-order approximation, one can use $\partial_t A(t) \approx (A(t) - A(t-\tau))/\tau$, where τ stands for the temporal mesh step. In this work, we use second-order approximation $\partial_t A(t) \approx (3A(t) - 4A(t-\tau) + A(t-2\tau))/2\tau$.

Therefore, in order to study pulse propagation along optical fibers, one should integrate numerically the following set of GNLSEs:

$$\partial_z A_{0,1} = \hat{D}A_{0,1} + \hat{N}A_{0,1} \tag{6}$$

for complex amplitudes of pump $A_0(z,t)$ and Stokes $A_1(z,t)$ waves, where $\hat{D}$ stands for linear terms of GNLSE (1), and $\hat{N}$ is defined by Eqs. (3) and (4). It is relevant to note that once dispersion coefficients $\beta_{k;0}$ ($k = 1, 2, 3, \ldots$) are known at the pump wavelength, they can be easily re-calculated for the Stokes wave: $\beta_{k;1} = \beta_{k;0} + \beta_{k+1;0}\omega_S + \beta_{k+2;0}\omega_S^2/2 + \ldots$. Numerical integration of simultaneous Eq. (6) can be done using SSFM or any other finite-difference methods applicable to "conventional" GNLSE (1). However, compared to the conventional approach where the pump and Stokes waves are simulated on a single mesh, the new model (6) allows one to achieve much higher efficiency due to substantial reduction of the mesh point count. Now let us compare the numerical results obtained using these two models and their efficiency.

3. NUMERICAL RESULTS AND DISCUSSION

As a test bed for the new model, we chose to simulate propagation of Fourier-limited Gaussian pulses with FWHM of 100 ps through a 100-m-long section of optical fiber with group velocity dispersion (GVD) $\beta_{2;0} = 14.44$ ps^2/km and $\beta_{3;0} = 0.045$ ps^3/km at pump wavelength $\lambda_0 = 1090$ nm and nonlinearity $\gamma = 4.7$ (W × km)$^{-1}$. The dispersion coefficients

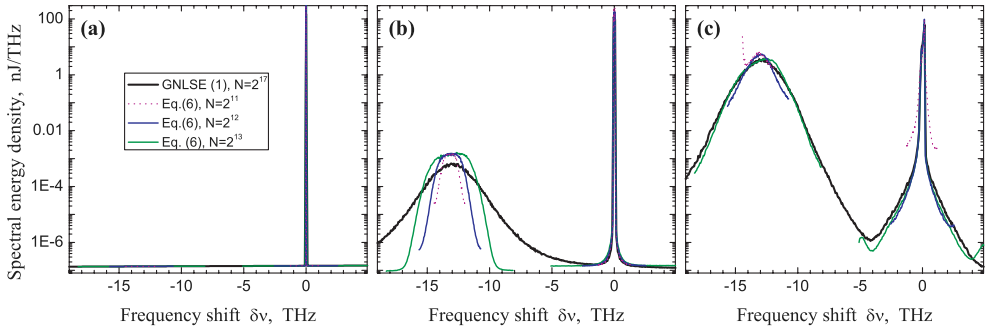

Fig. 1. Evolution of simulated optical spectra along optical fiber: (a) $z = 0$, (b) $z = 33.3$ m, (c) $z = 100$ m.

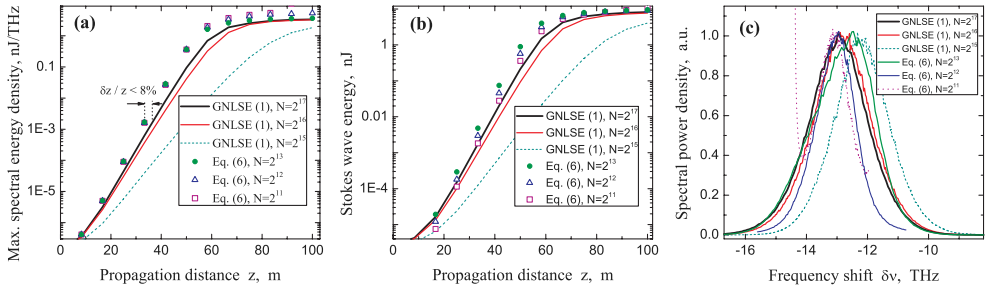

Fig. 2. (a) Maximal spectral energy density at Raman peak as a function of propagation distance z; (b) Stokes wave energy as a function of propagation distance z; (c) independently normalized spectra of Stokes wave at $z = 100$ m.

at Stokes wavelength $\lambda_1 = 1144.9$ nm are $\beta_{1;1} = -1.043$ ps/m, $\beta_{2;1} = 10.71$ ps^2/km, and $\beta_{3;1} = 0.045$ ps^3/km. The initial peak power of the pumping pulses is 158 W, which corresponds to the Raman threshold, i.e., the point where the pump and Stokes wave powers are equal at the exit of the fiber.

For numerical integration of Eq. (1), we used a uniform mesh with the number of points ranging from 2^{15} up to 2^{17}, whereas for integration of Eq. (6), a couple of meshes were used with the number of points varying from 2^{11} up to 2^{13}. The width of all meshes was 800 ps. Since the numerical solutions are obtained on temporal meshes with different numbers of points and a fixed width of 800 ps, the corresponding frequency meshes have different widths, as is clearly seen in Fig. 1 showing the optical spectrum evolution along the fiber. The initial conditions [Fig. 1(a)] are a superposition of a narrowband pump pulse and one photon with random phase in each frequency mesh point. This allows us to take into account spontaneously emitted quantum noise that seeds Raman amplification [30]. The numerical solutions shown in Fig. 1 are averaged over 50 random realizations of quantum noise. As the pumping pulse propagates along the optical fiber, its spectral peak (at $\delta\nu = 0$) broadens due to self-phase modulation, while the Raman peak appears and grows at $\delta\nu \approx -13$ THz according to numerical solution of GNLSE (1) [see black curve in Figs. 1(b) and 1(c)]. Similar behavior can be seen for two-component numerical solutions of the system (6) shown with red, blue, and green curves corresponding to $N = 2^{11}$, 2^{12}, and 2^{13} temporal mesh points, respectively. However, there are several clearly visible differences: the Stokes peak generated within the model (6) is narrower and higher [especially at $z = 33$ m; see Fig. 1(b)] than the one predicted by GNLSE (1). As well, emergence of instability can be seen at $z = 100$ m in numerical solution of (6) built with $N = 2^{11}$ temporal mesh points [see red curve in Fig. 1(c) at $\delta\nu \approx -14.4$ THz]. This is a numerical artifact that precludes using a very small number of mesh points.

In order to compare the results obtained within models (1) and (6) in more detail, it is instructive to consider Fig. 2(a) showing the height of the Stokes spectral peak as a function of propagation distance z of the pumping pulse. After a certain short initial transient period, the Stokes peak grows exponentially [linearly in log scale in Fig. 2(a)]; however, the growth rate predicted by Eq. (6) is slightly higher (by $\sim 7 \ldots 8\%$) than that given by GNLSE (1). It should be equally remembered that numerical results obtained with GNLSE (1) may also differ from each other if the number of mesh points N is not sufficiently large. Thus, the results obtained for $N = 2^{18}$ (not shown in order to avoid overcomplicating Fig. 2) and $N = 2^{17}$ virtually coincide differing from each other by less than 1%, which allows us to treat the latter solution as "exact" for the purposes of our study. Using it as a reference, we can estimate accuracy of the numerical solution obtained using $N = 2^{16}$ mesh points at about 7%, and for $N = 2^{15}$, at $\sim$30%. After $z \approx 50$ m, Raman conversion slows down because of pump depletion and a growing walk-off between pump and Stokes pulses due to GVD. Finally, by $z \approx 80$ m, the Raman peak virtually ceases to grow, as can be seen in Fig. 2(a) in all simulations except the case of GNLSE (1) with insufficient mesh point number $N = 2^{15}$.

Similar conclusions are valid for the energy of the Stokes wave evaluated as the integral of the energy density within a 20-THz-wide spectral range centered at $\omega_S/2\pi = -13$ THz [see Fig. 2(b)]. Unlike the Raman peak height dynamics shown in Fig. 2(a), Fig. 2(b) indicates slightly wider discrepancy in

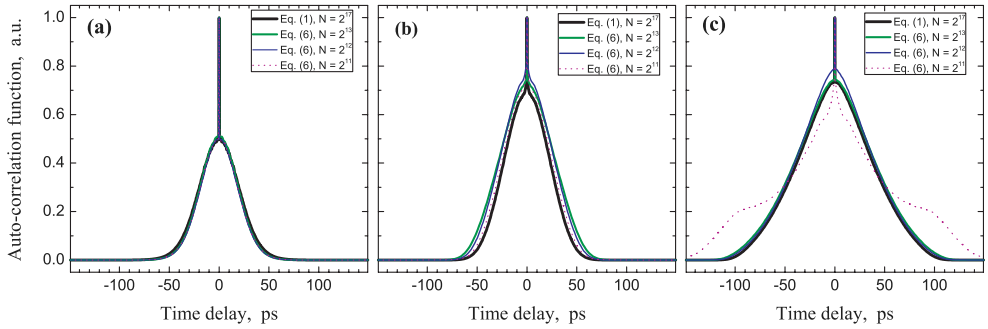

Fig. 3. Evolution of intensity ACF of Stokes wave along optical fiber: (a) $z = 33.3$ m, (b) $z = 66.7$ m, (c) $z = 100$ m.

the rate of exponential growth evaluated with a large number of points $N = 2^{13}$ due to overestimated spectral width shown earlier in Fig. 1(b). However, the discrepancy of the Stokes energy growth rate is 10% or less in all studied cases $N = 2^{11}$, 2^{12}, and 2^{13} as compared to that obtained using GNLSE (1) with $N = 2^{18}$ mesh points.

Besides the Raman peak height and energy, another important aspect of simulations is the optical spectrum of the Stokes wave. Spectra obtained in different simulations after propagation distance $z = 100$ m along optical fiber are shown in Fig. 2(c) after normalization to unity. It can be seen that all spectra have a similar shape except one obtained with the use of Eq. (6) with $N = 2^{11}$ mesh points, which shows an instability at the low-frequency boundary of the Stokes mesh. It is obvious in Fig. 2(c) that $N = 2^{11}$ mesh points is insufficient since the frequency mesh width in this case is narrower than the Stokes wave spectrum that is to be reproduced. The spectrum obtained by using Eq. (6) with $N = 2^{12}$ is still by 40% narrower, whereas the spectrum simulated with $N = 2^{13}$ mesh points is by 9% wider than the "quasi-exact" numerical solution of GNLSE (1) obtained with $N = 2^{17}$ mesh points.

It is pertinent to point out that qualitatively similar dynamics, including exponential initial growth of a Stokes wave with further saturation, was observed in early experiments with single-pass Raman conversion [31]. Although a detailed quantitative comparison with such experiments is challenging due to differences in pump and fiber parameters, one can surmise that certain features in spectral shape and dynamics reported in Ref. [31] cannot be reproduced here due to the Lorentzian approximation of the Raman response function (2). In cases when such spectral peculiarities are important, a more sophisticated model of Raman gain should be considered [32]. However, nowadays synchronously pumped Raman converters and lasers are used in most cases instead of single-pass configurations, resulting in much higher efficiency and lower noise. The Stokes wave feedback generates narrower optical spectra, therefore making more accurate the single-vibrational-mode approximation (2) as well as the approximation of slowly varying amplitudes, which both underpin the proposed model. Thus, one may expect further improvement of the model precision once intra-cavity Raman conversion is used instead of the single-pass configuration chosen here as a test bed for the new model.

Finally, let us inspect temporal intensity distributions of a simulated Raman pulse. Since the Stokes wave appears as a result of quantum noise amplification, the Stokes-shifted pulse at the beginning of Raman conversion can be considered as a weak stochastic replica of the pump pulse shortened due to the nonlinear nature of the Raman process, which is corroborated by numerical results obtained using both GNLSE (1) and the proposed model (6). However, the stochastic nature of Raman pulses and their complex noise-like structure complicate direct comparison of results generated by different models and with different meshes. In order to perform such a comparison, we plot intensity auto-correlation functions (ACFs) averaged over 100 random realizations of quantum noise that seeds the Raman process [see Fig. 3]. As can be seen in Fig. 3(a), at $z = 33.3$ m, the Stokes wave has a double-scale ACF shape indicating the noise-like structure of the Raman pulse. ACFs of the Stokes wave obtained in numerical simulations within Eqs. (1) and (6) virtually coincide for all used meshes. As the pump and Stokes waves propagate further along the fiber, the Raman pulse grows wider and gradually improves its degree of coherence, as indicated by a decreasing ACF central peak height. At $z = 66.7$ m, the results obtained within GNLSE (1) and Eq. (6) demonstrate a visible difference in the ACF pedestal width (up to 15%) and coherence peak height (up to 0.07). As seen in Fig. 3(b), Eq. (6) predicts faster growth of the pulse width and coherence similar to the above-mentioned faster energy transfer shown in Figs. 2(a) and 2(b). Finally, at $z = 100$ m, the difference in pulse width becomes less than 5%, and ACF coherence peak difference is 0.05 [see Fig. 3(c)]. The only exception is the numerical solution obtained using Eq. (6) with $N = 2^{11}$ mesh points, which demonstrates substantial distortion of ACF shape, which may be attributed to instability shown earlier in Figs. 1(c) and 2(c).

4. CONCLUSION

In conclusion, we proposed and tested a novel numerical model for nonlinear propagation of long laser pulses through optical fibers that takes into account chromatic dispersion, Kerr nonlinearity, and spectrally non-uniform Raman gain. In contrast to the conventional GNLSE, the proposed model generates a two-component numerical solution with two distinct slowly varying complex amplitudes for pump and Stokes waves instead of single complex amplitude in GNLSE. This allows reduction in the number of mesh points and results in a factor of 4…8 improvement in calculation speed and memory consumption at the expense of about 10% inaccuracy in the Stokes wave energy growth rate and less than 15% inaccuracy in the pulse duration,

as compared to the GNLSE solution. It should be emphasized that this level of inaccuracy is comparable to precision of the widely used GNLSE with a Lorentzian approximation of Raman response function (2), which was treated as "exact" for the purposes of this study [33]. Further reduction of the number of mesh points and a corresponding improvement in calculation speed and memory usage were impossible in the reported numerical tests due to the fact that the frequency mesh size became narrower than the Raman frequency peak. Nevertheless, further improvement may still be expected in the case of narrower generated spectra, e.g., due to spectral filtering, cavity feedback, or in the case of P_2O_5-doped fibers. The latter have a relatively narrow phosphorus Raman peak and a larger Stokes frequency shift. This may extend the model applicability into broader pump spectra and may further improve the model precision. Such cases will be the subject of further study.

Funding. Russian Foundation for Basic Research and Novosibirsk Oblast (19-42-540013).

Disclosures. The authors declare no conflicts of interest.

REFERENCES

1. G. P. Agrawal, *Nonlinear Fiber Optics* (Academic, 2007).
2. R. W. Boyd, *Nonlinear Optics* (Academic, 2003).
3. K. Blow and D. Wood, "Theoretical description of transient stimulated Raman scattering in optical fibers," IEEE J. Quantum Electron. **25**, 2665–2673 (1989).
4. A. E. Bednyakova, D. S. Kharenko, and A. P. Yarovikov, "On modelling of NPE mode-locked fiber laser in presence of Raman scattering," in *Conference on Lasers and Electro-Optics Europe and European Quantum Electronics Conference* (Optical Society of America, 2019), paper cj_p_60.
5. F. Copie, S. Randoux, and P. Suret, "The physics of the one-dimensional nonlinear Schrödinger equation in fiber optics: rogue waves, modulation instability and self-focusing phenomena," Rev. Phys. **5**, 100037 (2020).
6. I. Begleris and P. Horak, "Frequency-banded nonlinear Schrödinger equation with inclusion of Raman nonlinearity," Opt. Express **26**, 21527–21536 (2018).
7. B. N. Nyushkov, A. V. Ivanenko, S. M. Kobtsev, S. K. Turitsyn, C. Mou, L. Zhang, V. I. Denisov, and V. S. Pivtsov, "Gamma-shaped long-cavity normal-dispersion modelocked Er-fiber laser for sub-nanosecond high-energy pulsed generation," Laser Phys. Lett. **9**, 59–67 (2012).
8. S.-K. Wang, Q.-Y. Ning, A.-P. Luo, Z.-B. Lin, Z.-C. Luo, and W.-C. Xu, "Dissipative soliton resonance in a passively mode-locked figure-eight fiber laser," Opt. Express **21**, 2402–2407 (2013).
9. H. Lin, C. Guo, S. Ruan, and J. Yang, "Dissipative soliton resonance in an all-normal-dispersion Yb-doped figure-eight fibre laser with tunable output," Laser Phys. Lett. **11**, 085102 (2014).
10. K. Krzempek, "Dissipative soliton resonances in all-fiber Er-Yb double clad figure-8 laser," Opt. Express **23**, 30651–30656 (2015).
11. D. V. Churkin, S. Sugavanam, N. Tarasov, S. Khorev, S. V. Smirnov, S. M. Kobtsev, and S. K. Turitsyn, "Stochasticity, periodicity and localized light structures in partially mode-locked fibre lasers," Nat. Commun. **6**, 7004 (2015).
12. A. Ivanenko, S. Kobtsev, S. Smirnov, and A. Kemmer, "Mode-locked long fibre master oscillator with intra-cavity power management and pulse energy >12 μJ," Opt. Express **24**, 6650–6655 (2016).
13. D. S. Kharenko, V. D. Efremov, and S. A. Babin, "Study on harmonic generation regimes of Raman dissipative solitons in an external fibre cavity in a spectral region of 1.3 μm," Quantum Electron. **49**, 657–660 (2019).
14. H. Chen, S.-P. Chen, Z.-F. Jiang, K. Yin, and J. Hou, "All-fiberized synchronously pumped 1120 nm picosecond Raman laser with flexible output dynamics," Opt. Express **23**, 24088–24096 (2015).
15. K. Smith, P. Kean, D. Crust, and W. Sibbett, "An experimental study of a synchronously pumped fibre Raman oscillator," J. Mod. Opt. **34**, 1227–1233 (1987).
16. C. Aguergaray, A. Runge, M. Erkintalo, and N. G. R. Broderick, "Raman-driven destabilization of mode-locked long cavity fiber lasers: fundamental limitations to energy scalability," Opt. Lett. **38**, 2644–2646 (2013).
17. A. F. J. Runge, C. Aguergaray, N. G. R. Broderick, and M. Erkintalo, "Raman rogue waves in a partially mode-locked fiber laser," Opt. Lett. **39**, 319–322 (2014).
18. A. F. J. Runge, N. G. R. Broderick, and M. Erkintalo, "Observation of soliton explosions in a passively mode-locked fiber laser," Optica **2**, 36–39 (2015).
19. A. Kokhanovskiy, A. Ivanenko, S. Kobtsev, S. Smirnov, and S. Turitsyn, "Machine learning methods for control of fibre lasers with double gain nonlinear loop mirror," Sci. Rep. **9**, 2916 (2019).
20. D. S. Kharenko, E. V. Podivilov, A. A. Apolonski, and S. A. Babin, "20 nJ 200 fs all-fiber highly chirped dissipative soliton oscillator," Opt. Lett. **37**, 4104–4106 (2012).
21. C. Headley and G. P. Agrawal, "Unified description of ultrafast stimulated Raman scattering in optical fibers," J. Opt. Soc. Am. B **13**, 2170–2177 (1996).
22. B. Behzadi, M. Aliannezhadi, M. Hossein-Zadeh, and R. K. Jain, "Design of a new family of narrow-linewidth mid-infrared lasers," J. Opt. Soc. Am. B **34**, 2501–2513 (2017).
23. M. Aliannezhadi, F. Shahshahani, and V. Ahmadi, "Modeling the optical nonlinear effects on DFB-RF laser based on the transfer matrix method," Appl. Math. Modell. **74**, 85–93 (2019).
24. O. Batjargal, Y.-H. Ou, K. Keikens, J. K. Barton, and K. Kieu, "All-fiber dissipative soliton Raman laser based on phosphosilicate fiber," IEEE Photon. Technol. Lett. **30**, 1846–1849 (2018).
25. W. Pan, L. Zhang, J. Zhou, X. Yang, and Y. Feng, "Raman dissipative soliton fiber laser pumped by an ASE source," Opt. Lett. **42**, 5162–5165 (2017).
26. S. A. Babin, E. V. Podivilov, D. S. Kharenko, A. E. Bednyakova, M. P. Fedoruk, V. L. Kalashnikov, and A. Apolonski, "Multicolour nonlinearly bound chirped dissipative solitons," Nat. Commun. **5**, 4653 (2014).
27. X. Yang, L. Zhang, H. Jiang, T. Fan, and Y. Feng, "Actively mode-locked Raman fiber laser," Opt. Express **23**, 19831–19836 (2015).
28. A. E. Bednyakova, S. A. Babin, D. S. Kharenko, E. V. Podivilov, M. P. Fedoruk, V. L. Kalashnikov, and A. Apolonski, "Evolution of dissipative solitons in a fiber laser oscillator in the presence of strong Raman scattering," Opt. Express **21**, 20556–20564 (2013).
29. D. Churin, J. Olson, R. A. Norwood, N. Peyghambarian, and K. Kieu, "High-power synchronously pumped femtosecond Raman fiber laser," Opt. Lett. **40**, 2529–2532 (2015).
30. R. Smith, "Optical power handling capacity of low loss optical fibers as determined by stimulated Raman and Brillouin scattering," Appl. Opt. **11**, 2489–2494 (1972).
31. R. H. Stolen, C. Lee, and R. K. Jain, "Development of the stimulated Raman spectrum in single-mode silica fibers," J. Opt. Soc. Am. B **1**, 652–657 (1984).
32. D. Hollenbeck and C. D. Cantrell, "Multiple-vibrational-mode model for fiber-optic Raman gain spectrum and response function," J. Opt. Soc. Am. B **19**, 2886–2892 (2002).
33. Q. Lin and G. P. Agrawal, "Raman response function for silica fibers," Opt. Lett. **31**, 3086–3088 (2006).